nature physics

LETTERS

https://doi.org/10.1038/s41567-022-01721-w

Check for updates

Many-body dynamical delocalization in a kicked one-dimensional ultracold gas

Jun Hui See Toh[1], Katherine C. McCormick[1], Xinxin Tang[1], Ying Su[2], Xi-Wang Luo[2], Chuanwei Zhang[2] ✉ and Subhadeep Gupta[1] ✉

Contrary to a driven classical system that exhibits chaotic behaviour and diffusive energy growth, a kicked quantum system can exhibit the emergence of dynamical localization, which limits energy absorption and leads to the breakdown of ergodicity[1–4]. The evolution of dynamically localized states in the presence of many-body interactions has long remained an open question[5–7]. Here we experimentally study an interacting one-dimensional ultracold gas periodically kicked by a pulsed optical lattice and observe the interaction-driven emergence of dynamical delocalization and many-body quantum chaos. The observed dynamics feature sub-diffusive energy growth over a broad parameter range of interaction and kick strengths. These results shed light on interaction-driven transport phenomena in quantum many-body systems, in a regime where theoretical approaches are extremely challenging and provide conflicting predictions.

The classical kicked rotor is a textbook paradigm to explore chaos phenomena, displaying a diffusively growing kinetic energy proportional to time or kick number, above a critical kick strength[8,9]. Dynamical localization in the quantum kicked rotor (QKR)[1,2] arises from quantum interference, and can be explained by mapping[3,10] the Floquet dynamics of the QKR to a disordered Anderson model[11] in the momentum-space lattice. In the past three decades, single-particle QKRs have been experimentally studied extensively with cold neutral atoms and dynamical localization has been observed[4,12–18].

Understanding the role of many-body interactions in a disordered quantum system has been a long-standing challenge since the discovery of Anderson localization[11]. In recent years, many-body localization in disordered lattices in position space has been extensively studied both experimentally and theoretically by incorporating methods developed in quantum information science[19–21]. Despite the equivalence of dynamical localization[3,10] to Anderson localization[11] for a single particle, the infinite long-range interaction in the momentum-space lattice is fundamentally different from the short-range interaction in position-space Anderson lattices[19–22], posing a major obstacle for understanding many-body effects in dynamical localization[5–7,23–27]. In fact, conflicting theoretical predictions exist: although mean-field calculations for interacting Bose–Einstein condensates (BECs) predict delocalization in momentum space with a sub-diffusive character[5,6] (that is, weaker-than-linear growth of system energy), the low-energy approximation based on Luttinger liquid theory of a kicked one-dimensional (1D) Lieb–Liniger gas shows the persistence of dynamical localization[7].

Here we perform the first experimental study of many-body effects in the dynamical localization of a QKR and report the observation of an interaction-driven transition between dynamically localized and delocalized states. In our periodically kicked 1D bosonic system with contact interactions, the delocalization is evident as a clear onset of sub-diffusive energy growth with kick number as the interaction is strengthened through tight transverse confinement. The sub-diffusive behaviour persists over a range of interaction strengths and kick parameters. Our theoretical modelling with mean-field and Hartree–Fock–Bogoliubov (HFB) approaches reasonably capture the observed dynamics in the deep delocalization and localization regions. However, the mean-field theory fails across the phase transition boundary, potentially due to strong competition between the disorder potential and interaction-induced infinite long-range coupling in the momentum-space lattice, which is extremely challenging to model in theory.

We initiate our experiments (Methods and Supplementary Information provide more experimental and theoretical details) by preparing an essentially pure three-dimensional (3D) BEC containing 1.5×10^5 atoms of ^{174}Yb with chemical potential $h\times1.1$ kHz in an optical dipole trap (ODT) and subsequently loading it into a two-dimensional optical lattice where the atoms reside in a set of 1D tubes with negligible intertube tunnelling (Fig. 1a). The starting BEC fraction in the tubes is higher than 85%. The kicks are implemented by a pulsed one-dimensional optical lattice along the axial direction of the tubes. Each of the three orthogonal lattices is formed from retro-reflected laser beams ($\simeq$100 μm waist) and has a spatial period of 1,073 nm/2 $=\pi/k_L$ with corresponding recoil energy $E_{rec}=\hbar\omega_{rec}$, where $\omega_{rec}=\hbar k_L^2/2m=2\pi\times1$ kHz; m is the atom mass; k_L is the wavenumber; $\hbar$ is the reduced Planck constant. The kick parameters are tunable through the kick period T, pulse width t_p and potential depth s_zE_{rec}. Each of the two transverse lattices has depth $s_\perp E_{rec}$. For the typical $s_\perp=106$ used in this work, the transverse trap frequency (for the central tube) is $\omega_\perp=2\sqrt{s_\perp}\,\omega_{rec}=2\pi\times20.5$ kHz. The transverse oscillator length is $a_\perp=\sqrt{\hbar/m\omega_\perp}\simeq53$ nm, and the axial frequency is $\omega_z=2\pi\times64$ Hz. From the Thomas–Fermi (TF) radii of the 3D trap and the measured axial size in the 1D tubes, we estimate a peak particle number of $N_{atom}=650$ and an initial 1D peak density of $\bar{n}_{1D}=24\,\mu m^{-1}$ for the central tube.

We monitor the system by diabetically turning off all the optical potentials after a desired number (n_p) of kicks and then taking a time-of-flight absorption image from which we extract the atomic momentum distribution in both axial and transverse directions. The measured transverse distribution is consistent with the transverse ground-state energy (Fig. 1b). The 1D geometry with $\omega_\perp\gg\omega_{rec}$ suppresses two-body scattering from the axial to the transverse directions, as evident in the negligible growth of transverse energy $\langle E_\perp\rangle$ during the kicking process (Fig. 1b) for $s_\perp\geq20$. As interactions are

[1]Department of Physics, University of Washington, Seattle, WA, USA. [2]Department of Physics, The University of Texas at Dallas, Richardson, TX, USA. ✉e-mail: Chuanwei.Zhang@utdallas.edu; deepg@uw.edu

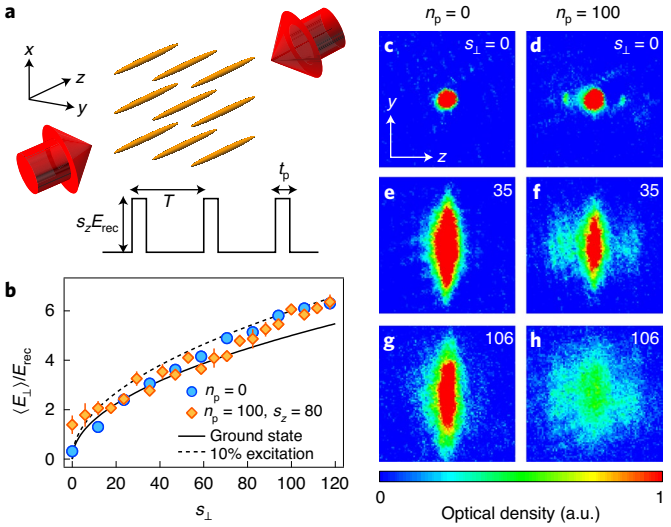

Fig. 1 | Experimentally realizing the interacting 1D QKR system. **a**, Experimental schematic showing BECs in 1D tubes with periodic kicking pulses applied along the axial (z) direction. **b**, Average transverse energy $\langle E_\perp \rangle$ for various $s_\perp$ values for no kick (circles) and 100 kicks with $s_z = 80$ and $(t_p, T) = (2, 105)$ μs (diamonds). The solid line indicates the calculated energy for the transverse ground state and the dashed line indicates that for 10% occupation of the first transverse excited state. The error bars show 1 standard error of the mean (s.e.m.; not visible when smaller than the marker size). **c**–**h**, Time-of-flight atom absorption images after 0 (**c**, **e** and **g**) and 100 (**d**, **f** and **h**) kicks for $s_\perp = 0$ (3D case) and $s_\perp = 35$ and 106. For **d**, **f** and **h**, $s_z = 80$ and $(t_p, T) = (2, 105)$ μs. The imaging axis is along the x direction and each image spans the momentum range $10\hbar k_L \times 10\hbar k_L$.

increased by raising $s_\perp$, the axial (z) momentum width after many pulses also increases ($n_p = 0$, 100; Fig. 1c–h), providing a key signature for examining the many-body QKR.

Even though condensation is not possible in the homogeneous 1D case[28–30], axial harmonic confinement supports BEC[31]. For our experimental parameters, the system is quasi-1D where the gas is kinematically 1D with the two-body scattering length $a_s = 5.55$ nm ($\ll a_\perp$), retaining its 3D value. The correlation length $l_c = \hbar/\sqrt{m\bar{g}\bar{n}_{1D}}$ is much larger than the mean interparticle separation $1/\bar{n}_{1D}$, which makes the ground state of the initial system a true TF condensate[32]. Here $\bar{g} = 2\hbar^2 a_s/(ma_\perp^2)$ is the mean-field interaction constant.

We model the many-body dynamics of bosons with the mean-field theory, where the QKR wavefunction Φ is governed by the nonlinear Gross–Pitaevskii (GP) equation:

$$i\bar{k}\partial_\tau \Phi(\theta,\tau) = \left(-\frac{\bar{k}^2}{2}\partial_\theta^2 - K\cos\theta \sum_{n_p} \delta(\tau - n_p) + \frac{1}{2}\omega_\theta^2\theta^2 + g|\Phi(\theta,\tau)|^2 \right)\Phi(\theta,\tau) \quad (1)$$

where $\theta = 2k_L z$ and $\tau = t/T$ are dimensionless parameters, and $\bar{k} = 8\omega_{rec}T$ is the dimensionless effective Planck constant. The dimensionless kick strength K and interaction constant g are defined as

$$K = 4s_z\omega_{rec}^2 t_p T, \quad g = \frac{2\bar{g}k_L\bar{k}T}{\hbar} = \bar{k}^2\frac{k_L a_s}{(k_L a_\perp)^2}. \quad (2)$$

The dimensionless axial frequency is $\omega_\theta = \omega_z T$ and the dimensionless initial peak density is $n_{1D} = |\Phi(0,0)|^2 = \bar{n}_{1D}/2k_L$, where the wavefunction is normalized as $\int d\theta |\Phi(\theta,\tau)|^2 = N_{atom}$. We control the interaction strength gn_{1D} through the transverse confinement of the 1D tubes; throughout this Letter, the quoted interaction strength is an average value that takes into account the variation in the atom number in different tubes. When the two-dimensional lattice is off, the BEC resides purely in the ODT and has the weakest interaction strength. In this case, the system is 3D and we obtain an effective 1D interaction strength gn_{1D}^{eff} by adjusting $a_\perp$ (equation (2)) to match the measured chemical potential of the BEC in the ODT.

We first discuss QKR experiments on a 3D system, implemented by applying the pulsed lattice on the BEC trapped in the ODT with no transverse lattice. Here we always observe dynamical localization (Fig. 2a,c,e,g), consistent with weak interactions. Following some initial coherent dynamics, the momentum distribution and mean energy $\langle E_z \rangle$ quickly saturate. Compared with the exponentially localized function $e^{-|p|/\xi}$, the observed momentum profile exceeds the expected dynamical localization length $\xi = K^2/4\bar{k}^2 = 0.25$ (in units of $\hbar k_L$) for a non-interacting system, but is better contained by $\xi = 0.92$ corresponding to the observed saturated value $\langle E_z \rangle = 1.7E_{rec}$ (Fig. 2c–f, dashed and dotted lines). Although the momentum distribution is clearly localized at long times, its asymptotic shape has peaks at $\pm 2\hbar k_L$. The exponential functions serve only to allow comparison against the non-interacting case, with the observed deviations stemming from the small but non-zero g and the narrow initial momentum width compared with $2\hbar k_L$. In striking contrast to the 3D case, many-body dynamical delocalization is evident for higher interaction strengths available in the 1D geometry, with sub-diffusive energy growth (Fig. 2b,d,f,g).

Figure 3 shows a study of the delocalization behaviour for different kick strengths K (tuned through s_z) and interaction strengths (tuned through $s_\perp$). The dynamics are strongly dependent on K (Fig. 3a), with the earliest onset of delocalization for $(gn_{1D}, K) = (18.7, 5.3)$ exhibiting substantial energy growth even within the first ten pulses. We note that this timescale (1 ms) is more than ten times shorter than the axial oscillation period, indicating that harmonic confinement along the tube is not a prerequisite for the observed delocalization. As K is lowered, the onset time of delocalization is delayed, extending to nearly 100 pulses for the lowest K. This is also evident in Fig. 3b which corresponds to a vertical cut of the data in Fig. 3a (fixed $n_p = 15$ and $gn_{1D} = 18.7$) and shows the monotonic growth of the mean axial energy with K.

We investigate the dependence of delocalization behaviour on the interaction strength by changing the external confinement through $s_\perp$, which changes $a_\perp$ and hence g and n_{1D}. As shown in Fig. 3c, we find stronger delocalization with higher gn_{1D} for fixed $K = 2.6$, with only the lowest $gn_{1D}^{eff} = 3.9$ case remaining localized. This is also evident in Fig. 3d, which corresponds to a vertical cut of the data in Fig. 3c (fixed $n_p = 100$ and $K = 2.6$) and shows the monotonic growth of the mean axial energy with gn_{1D}.

To compare with earlier theoretical results of interaction-driven sub-diffusive energy evolution in the QKR[6,24], we fit our delocalization data using power-law functions $E_0\tau^\alpha$ to $\langle E_z \rangle$ (Fig. 3a,c, black solid lines). The finite trap depth results in atom loss for $\langle E_z \rangle$ above $10E_{rec}$ (Methods and Supplementary Information provide more experimental and theoretical details) and the axial oscillation period introduces an additional timescale to the QKR. Restricting attention to the delocalization data with $\langle E_z \rangle$ below $10E_{rec}$ and evolution time below the axial period, our fit results for α lie in the range of 0.36–0.80. This observed sub-diffusivity is intermediate between classical chaotic behaviour and single-particle quantum mechanics and signals the fundamentally distinct dynamics of a driven quantum many-body system. Our α values are somewhat larger than the predictions of 0.3–0.4 elsewhere[24] and more consistent with the 0.4–0.8 range predicted in another study[6]. Furthermore, we do not observe any obvious trend of α with K or gn_{1D}, which is also consistent with the numerical findings discussed elsewhere[6]. However, we do clearly observe a trend for the onset time of delocalization,

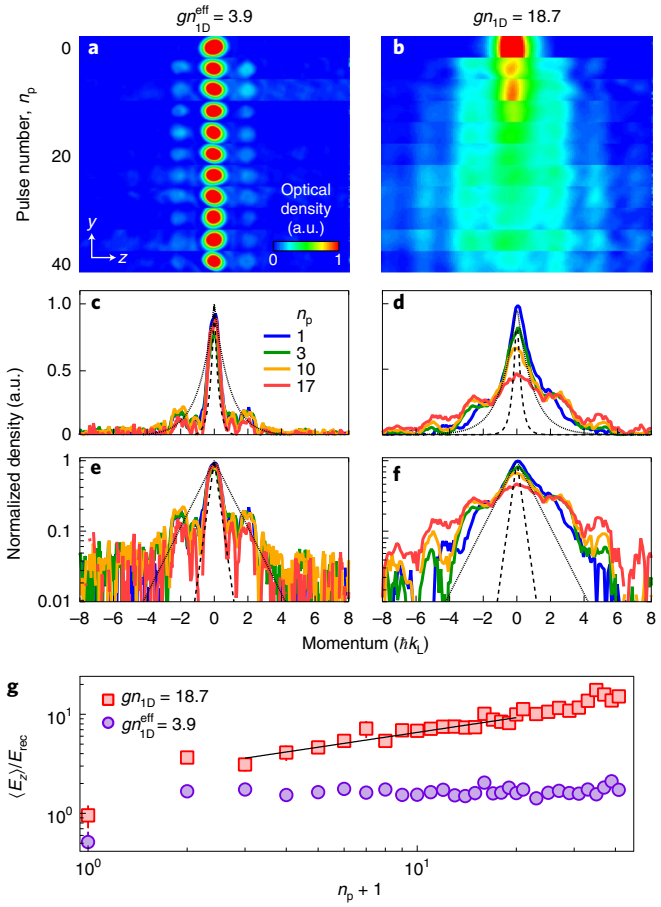

Fig. 2 | Momentum and energy evolution for dynamically localized and delocalized rotors. a,**b**, Sequences of absorption images for localized (**a**) and delocalized (**b**) cases with $\bar{k} = 5.26$, $K = 5.3$ and $(t_p, T) = (2, 105)$ μs. **c**,**d**, Axial momentum distributions after kick numbers $n_p = 1, 3, 10, 17$, corresponding to the data in **a** (**c**) and **b** (**d**), respectively. The dashed and dotted lines are exponential functions (see the main text). **e**,**f**, The same data as those in **c** (**e**) and **d** (**f**), shown on a logarithmic scale. **g**, Evolution of the axial kinetic energy corresponding to **a** and **b**. The solid line is a power-law fit to the delocalized data, returning an exponent value of 0.36. The error bars show 1 s.e.m. (not visible when smaller than the marker size). The $gn_{1D}^{eff} = 3.9$ data are obtained in the 3D system.

which decreases with an increase in either K or gn_{1D} (Methods and Supplementary Information provide more experimental and theoretical details).

We carry out numerical mean-field simulations of the dynamics (Fig. 3a,c, solid lines), starting from the TF ground state obtained by the imaginary time evolution of the GP equation (Methods and Supplementary Information provide more experimental and theoretical details). We find that for a given interaction strength gn_{1D}, the system enters a dynamically delocalized phase with mean energy increasing with pulse number when K is larger than a critical value K_c. As gn_{1D} increases, K_c decreases, implying that dynamical delocalization is easier for stronger interactions. The variation in K_c marks the boundary (Fig. 3e, solid line) between the localized and delocalized phases in the K–gn_{1D} parameter space. We see reasonable agreement between theory and experiment in the system time evolution for points deep in the delocalization and localization regimes. However, notable deviations between the two exist for points near the phase boundary.

The delocalization physics may be understood more intuitively in momentum space, where the non-interacting QKR can be mapped to a one-dimensional lattice with onsite disorders[3]. In momentum space, the real-space contact interaction introduces onsite nonlinear terms as well as infinite long-range nonlinear cross-hopping terms to the disordered lattice, which are responsible for dynamical delocalization (Methods and Supplementary Information provide more experimental and theoretical details). The observed failure of the mean-field approach near the phase boundary is, therefore, unsurprising since the dynamics near K_c are very sensitive to the competition between disorder and interaction-induced infinite long-range coupling in the momentum-space lattice. We also note that the finite momentum width of the initial state and interaction-induced scattering between the different momenta may lead to density peaks away from the recoil momenta ($2jk_L$ with integer j), which can happen at a small kick number for large K (Fig. 2).

Initially, our system is a true TF condensate with negligible fluctuations. As the kick number increases, the delocalization of the interacting system is accompanied by a rapid proliferation of non-condensate particles. The mean-field GP approach is valid only when quantum depletion is low, that is, the non-condensate fraction is much smaller than the condensed fraction. Going beyond the mean field, we examine the excitation properties by employing the HFB[5,33] (Methods and Supplementary Information provide more experimental and theoretical details) approximation to calculate the evolution of the non-condensate particle number $\langle \hat{\psi}^\dagger \hat{\psi} \rangle$, where $\hat{\psi}$ represents the quantum fluctuation beyond the condensate $\Phi(\theta, \tau)$. The dashed line in Fig. 3e represents the boundary between the stable and unstable regimes, where the unstable regime is evident as an exponential increase in the non-condensate particles with n_p. The two-phase boundaries (Fig. 3e, solid and dashed lines) are close to each other, suggesting that the dynamical delocalization is accompanied by BEC instability.

We find that the interaction-driven delocalization is a general feature of our system (Methods and Supplementary Information provide more experimental and theoretical details) as we observe it for various values of kick period T ranging from 20 to 125 μs. Furthermore, apart from using transverse confinement, we have also controlled the interaction strength by varying the number of atoms loaded into the tubes and observed similar interaction-driven delocalization.

Our results experimentally realize the interacting QKR, a long-sought quantum-mechanical paradigm system. The combined experimental and theoretical study of many-body localized and delocalized phases in momentum space spotlight the emergence of many-body quantum chaos (that is, many-body effects on a quantum system where the corresponding classical system may exhibit chaos) and constitute the first study of the effects of interactions on dynamical localization, an area where current theoretical results are in conflict[5–7]. Direct extensions of these studies include further characterizations of the boundary between localized and delocalized phases where we observe the mean-field theory to fail, of the onset time of delocalization and of the sub-diffusive delocalization exponent[6,24]. It will also be interesting to extend the current implementation carried out with $\gamma = 1/(l_c \bar{n}_{1D})^2 \ll 1$ into the $\gamma \gg 1$ Tonks–Girardeau regime[34,35], where beyond-mean-field theories predict many-body dynamical localization with momentum profile distinct from their spatially localized counterpart[7,26,27]. Our technique of tight confinement to tune interactions in the synthetic momentum space can also be extended towards studies of the momentum-space Josephson effect[36], interaction-driven transport in higher synthetic dimensions[37,38] and topological phases with interactions in coupled momentum-space lattices[39].

During the course of this work, we became aware of related results from another experimental group[40]. Although this other

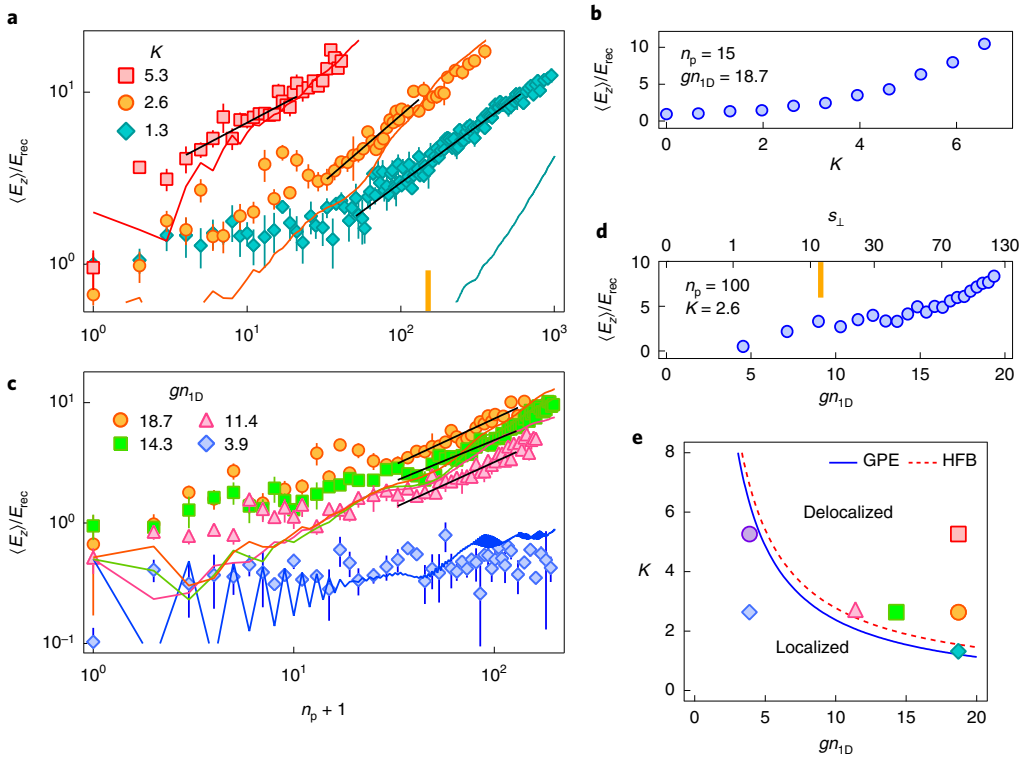

Fig. 3 | Tuning the onset of many-body quantum chaos with interaction and kick strengths. For all the data in this figure, $(t_p, T) = (2, 105)\,\mu s$ and $\bar{k} = 5.26$. **a**, Evolution of $\langle E_z \rangle$ with pulse number for three different kick strengths and fixed $gn_{1D} = 18.7$. The yellow vertical bar indicates the axial oscillation period. The coloured solid lines are the corresponding numerical simulations using the GP equation. The black solid lines are power-law fits to the delocalized data, which return the exponent values of $\{0.36, 0.79, 0.67\}$ for $K = \{5.3, 2.6, 1.3\}$. **b**, $\langle E_z \rangle$ after 15 kicks for various K values and fixed $gn_{1D} = 18.7$. **c**, Evolution of $\langle E_z \rangle$ with pulse number for four different interaction strengths with $K = 2.6$. To preserve a similar axial trapping frequency for low $s_\perp$, the ODT is kept on for the data in **c** and **d**, except for the $gn_{1D} = 18.7$ data (orange circles). The $gn_{1D}^{eff} = 3.9$ data are obtained in the 3D system. The power-law fits (black solid lines) to the delocalized data return exponent values of $\{0.79, 0.67, 0.79\}$ for $gn_{1D} = \{18.7, 14.3, 11.4\}$. **d**, $\langle E_z \rangle$ after 100 kicks for various gn_{1D} values and fixed $K = 2.6$, where the yellow vertical bar marks the intertube tunnelling time of 21 ms ($n_p = 200$). **e**, Phase diagram of the localization–delocalization behaviour of the system for $\bar{k} = 5.26$, where the lines indicate the phase boundaries by solving the GP (solid) and HFB (dashed) equations. The filled markers correspond to the data from **a** and **c** as well as Fig. 2g. All the error bars in **a**–**d** show 1 s.e.m. (not visible when smaller than the marker size). The statistical errors on the fitted exponents are ≤13%.

work also realizes an interacting QKR using atomic BECs subjected to a series of pulsed optical standing waves, it is implemented in a substantially different parameter regime and utilizes complementary experimental techniques[40]. It uses ^{7}Li atoms—about 25 times lighter than the ^{174}Yb atoms used in the present work—leading to an order-of-magnitude faster kicked-rotor timescales. Secondly, atomic interactions are tuned using a magnetic Feshbach resonance[40], in contrast to the tuning through density variation used in the present work. Finally, all the experiments in that study[40] are performed using a 3D condensate rather than the 1D system used in the present work. Despite these differences, both experiments demonstrate interaction-induced dynamical delocalization, with a sub-diffusive temporal evolution of energy. Taken together, these results establish a new testbed for investigating interaction-driven transport phenomena and many-body quantum chaos.

Online content

Any methods, additional references, Nature Research reporting summaries, source data, extended data, supplementary information, acknowledgements, peer review information; details of author contributions and competing interests; and statements of data and code availability are available at https://doi.org/10.1038/s41567-022-01721-w.

Received: 8 October 2021; Accepted: 14 July 2022;
Published online: 26 September 2022

References

1. Casati, G., Chirikov, B. V., Izraelev, F. M. & Ford, J. Stochastic behavior of a quantum pendulum under a periodic perturbation. in *Stochastic Behavior in Classical and Quantum Hamiltonian Systems* 334–352 (Springer, 1979).
2. Lemarié, G. et al. Observation of the Anderson metal-insulator transition with atomic matter waves: theory and experiment. *Phys. Rev. A* **80**, 043626 (2009).
3. Fishman, S., Grempel, D. R. & Prange, R. E. Chaos, quantum recurrences, and Anderson localization. *Phys. Rev. Lett.* **49**, 509 (1982).
4. Moore, F. L., Robinson, J. C., Bharucha, C. F., Sundaram, B. & Raizen, M. G. Atom optics realization of the quantum δ-kicked rotor. *Phys. Rev. Lett.* **75**, 4598 (1995).
5. Zhang, C., Liu, J., Raizen, M. G. & Niu, Q. Transition to instability in a kicked Bose-Einstein condensate. *Phys. Rev. Lett.* **92**, 054101 (2004).
6. Lellouch, S., Rançon, A., De Bièvre, S., Delande, D. & Garreau, J. C. Dynamics of the mean-field-interacting quantum kicked rotor. *Phys. Rev. A* **101**, 043624 (2020).
7. Rylands, C., Rozenbaum, E. B., Galitski, V. & Konik, R. Many-body dynamical localization in a kicked Lieb-Liniger gas. *Phys. Rev. Lett.* **124**, 155302 (2020).
8. Lichtenberg, A. & Lieberman, M. *Regular and Chaotic Dynamics* (Springer, 1992).
9. Chirikov, B. V. A universal instability of many-dimensional oscillator systems. *Phys. Rep.* **52**, 263 (1979).

10. Grempel, D. R., Prange, R. E. & Fishman, S. Quantum dynamics of a nonintegrable system. *Phys. Rev. A* **29**, 1639 (1984).
11. Anderson, P. W. Absence of diffusion in certain random lattices. *Phys. Rev.* **109**, 1492 (1958).
12. Moore, F. L., Robinson, J. C., Bharucha, C., Williams, P. E. & Raizen, M. G. Observation of dynamical localization in atomic momentum transfer: a new testing ground for quantum chaos. *Phys. Rev. Lett.* **73**, 2974 (1994).
13. Ammann, H., Gray, R., Shvarchuck, I. & Christensen, N. Quantum delta-kicked rotor: experimental observation of decoherence. *Phys. Rev. Lett.* **80**, 4111 (1998).
14. d'Arcy, M. B. Godun, R. M., Oberthaler, M. K., Cassettari, D. & Summy, G. S. Quantum enhancement of momentum diffusion in the delta-kicked rotor. *Phys. Rev. Lett*. **87**, 074102 (2001).
15. Wimberger, S., Guarneri, I. & Fishman, S. Quantum resonances and decoherence for δ-kicked atoms. *Nonlinearity* **16**, 1381 (2003).
16. Duffy, G. J. et al. Experimental investigation of early-time diffusion in the quantum kicked rotor using a Bose-Einstein condensate. *Phys. Rev. E* **70**, 056206 (2004).
17. Ullah, A., Reddel, S., Currivan, J. & Hoogerland, M. D. Quantum resonant effects in the delta-kicked rotor revisited. *Eur. Phys. J. D* **66**, 315 (2012).
18. Gadway, B., Reeves, J., Krinner, L. & Schneble, D. Evidence for a quantum-to-classical transition in a pair of coupled quantum rotors. *Phys. Rev. Lett.* **110**, 190401 (2013).
19. Schreiber, M. et al. Observation of many-body localization of interacting fermions in a quasirandom optical lattice. *Science* **349**, 842–845 (2015).
20. Lukin, A. et al. Probing entanglement in a many-body–localized system. *Science* **364**, 256–260 (2019).
21. Abanin, D. A., Altman, E., Bloch, I. & Serbyn, M. Colloquium: many-body localization, thermalization, and entanglement. *Rev. Mod. Phys.* **91**, 021001 (2019).
22. Deissler, B. et al. Delocalization of a disordered bosonic system by repulsive interactions. *Nat. Phys.* **6**, 354–358 (2010).
23. Pikovsky, A. S. & Shepelyansky, D. L. Destruction of Anderson localization by a weak nonlinearity. *Phys. Rev. Lett.* **100**, 094101 (2008).
24. Flach, S., Krimer, D. O. & Skokos, C. Universal spreading of wave packets in disordered nonlinear systems. *Phys. Rev. Lett.* **102**, 024101 (2009).
25. Notarnicola, S., Silva, A., Fazio, R. & Russomanno, A. Slow heating in a quantum coupled kicked rotors system. *J. Stat. Mech.* **2020**, 024008 (2020).
26. Chicireanu, R. & Rançon, A. Dynamical localization of interacting bosons in the few-body limit. *Phys. Rev. A* **103**, 043314 (2021).
27. Vuatelet, V. & Rançon, A. Effective thermalization of a many-body dynamically localized Bose gas. *Phys. Rev. A* **104**, 043302 (2021).
28. Lieb, E. H. & Liniger, W. Exact analysis of an interacting Bose gas. I. The general solution and the ground state. *Phys. Rev.* **130**, 1605 (1963).
29. Lieb, E. H. Exact analysis of an interacting Bose gas. II. The excitation spectrum. *Phys. Rev.* **130**, 1616 (1963).
30. Yang, C. N. & Yang, C. P. Thermodynamics of a one-dimensional system of bosons with repulsive delta-function interaction. *J. Math. Phys.* **10**, 1115 (1969).
31. Ketterle, W. & Van Druten, N. J. Bose-Einstein condensation of a finite number of particles trapped in one or three dimensions. *Phys. Rev. A* **54**, 656 (1996).
32. Petrov, D. S., Shlyapnikov, G. V. & Walraven, J. T. M. Regimes of quantum degeneracy in trapped 1D gases. *Phys. Rev. Lett.* **85**, 3745 (2000).
33. Griffin, A. Conserving and gapless approximations for an inhomogeneous Bose gas at finite temperatures. *Phys. Rev. B* **53**, 9341 (1996).
34. Paredes, B. et al. Tonks–Girardeau gas of ultracold atoms in an optical lattice. *Nature* **429**, 277–281 (2004).
35. Kinoshita, T., Wenger, T. & Weiss, D. S. Observation of a one-dimensional Tonks-Girardeau gas. *Science* **305**, 1125–1128 (2004).
36. Hou, J. et al. Momentum-space Josephson effects. *Phys. Rev. Lett.* **120**, 120401 (2018).
37. Cherroret, N., Vermersch, B., Garreau, J. C. & Delande, D. How nonlinear interactions challenge the three-dimensional Anderson transition. *Phys. Rev. Lett.* **112**, 170603 (2014).
38. Vermersch, B., Delande, D. & Garreau, J. C. Bogoliubov excitations in the quasiperiodic kicked rotor: stability of a kicked condensate and the quasi–insulator-to-metal transition. *Phys. Rev. A* **101**, 053625 (2020).
39. Meier, E. J. et al. Observation of the topological anderson insulator in disordered atomic wires. *Science* **362**, 929–933 (2018).
40. Cao, A. et al. Prethermal dynamical localization and the emergence of chaos in a kicked interacting quantum gas. Preprint at https://arxiv.org/abs/2106.09698v1 (2021).

Methods

Experimental setup. The experiments discussed in this work were performed in an apparatus discussed in earlier work[41–43] and augmented with a set of three mutually orthogonal and independently controlled optical lattices. We prepare a BEC containing 1.5×10^5 atoms of ^{174}Yb atoms in a crossed ODT[42] with trapping frequencies $\{\omega_{0x},\omega_{0y},\omega_{0z}\}=2\pi\times\{145,16,53\}$ Hz, chemical potential $h\times1.1$ kHz and the corresponding TF radii of {2.4, 22, 6.6} μm. The BEC is then transferred into a two-dimensional optical lattice formed by two pairs of counterpropagating laser beams where the atoms reside in a set of 1D tubes (Fig. 1a). The lattice and kick optical potentials are derived from a home-built external cavity diode laser operated at a wavelength of $\lambda=1{,}073$ nm, and amplified by a 50 W amplifier (Nufern NUA-1064-PD-0050-D0). The total laser power for the lattice beams is distributed between three paths—two for the two-dimensional transverse optical lattice and one for the axial kicking lattice. To suppress optical interference between the different paths from affecting the atoms, for each pair of paths, we maintain orthogonal linear polarizations and use acousto-optic modulators to establish frequency separation greater than 40 MHz. The laser beams forming the two-dimensional transverse lattice are intensity stabilized at the 2% level. We calibrate the depth of our lattices using single-pulse Kapitza–Dirac diffraction, a procedure that also provides an experimental measurement of our lattice-beam waists to be $\{w_x,w_y,w_z\}=\{121,101,99\}$ μm, which are much larger than the BEC size.

Loading and characterizing the 1D gas. To transfer the BEC from the ODT to 1D confinement, the transverse lattice is ramped up exponentially in 100 ms with an exponential time constant of 20 ms. To assess the adiabaticity of this process, we performed tests in which the forward (loading) ramp is immediately followed by a reverse ramp back to the ODT after which we compare the final BEC fraction with the initial value. Starting from an essentially pure BEC, we obtain about 70% BEC fraction after the forward and reverse ramps, suggesting that the BEC fraction is about 85% in the two-dimensional lattice. We believe this number to be a lower bound because the recovered BEC fraction is probably also limited by the lack of coherence between the tubes, as tunnelling is strongly suppressed beyond $s_\perp\simeq20$.

The atoms are loaded into about 570 horizontal tubes, as determined by the initial TF radii in the 3D trap. We measure an initial (tube-averaged) axial size of 27 μm for $s_\perp=106$. The peak density of the central tubes is about $\bar{n}_{1D}=24\,\mu m^{-1}$. Once the BEC is loaded into the two-dimensional lattice, we exponentially ramp down the ODT in 50 ms with a time constant of 10 ms, before pulsing on the kick laser along the axial direction of the tubes. To obtain the momentum distribution, we diabetically turn off all the optical potentials and take an absorption image of the atoms after a long time of flight set to a value between 15 and 43 ms.

The observed growth rate of the axial momentum distribution in the absence of kicking pulses determines the background heating rate in the system. For $s_\perp=106$, we measure a kinetic-energy growth rate of $6E_{rec}\,s^{-1}$. All the QKR experiments reported in this work occur within 100 ms, a timescale during which this background heating is negligible. The calculated photon-scattering rate from the transverse lattice is $<0.1\,s^{-1}$ for $s_\perp=106$, suggesting that the observed residual heating is from technical noise.

Kicking-pulse implementation. The kick pulses are generated by triggering a function generator (Stanford Research Systems DS345) to produce a desired sequence of voltage pulses, which, in turn, controls the radio-frequency switch driving the acousto-optic modulator for the kicking-lattice laser beam. By integrating over the observed axial momentum distribution of the atoms in the time-of-flight absorption image, we calculate the kinetic energy delivered to the system by the kicks.

Nonlinear Anderson model in the momentum-space lattice. The QKR is a Floquet system with wavefunction $\Phi(\theta,\tau)=e^{-i\epsilon\tau}\phi(\theta,\tau)$, where $\phi(\theta,\tau)=\phi(\theta,\tau+1)$ is the periodic part and ϵ is the quasienergy. The δ-kick leads to $\phi_+(\theta)=e^{iK\cos(\theta)/\bar{k}}\phi_-(\theta)$, where $\phi_+(\theta)$ and $\phi_-(\theta)$ are the wavefunctions immediately after and before the kick, respectively. In the momentum-space lattice, the free evolution between kicks is described as

$$\begin{aligned} i\bar{k}\partial_\tau\phi_j(\tau) &= \left(\frac{\bar{k}^2j^2}{2}-\bar{k}\epsilon\right)\phi_j(\tau) \\ &+ \frac{g}{4\pi M}\left(2N_{\rm atom}-|\phi_j|^2\right)\phi_j(\tau) \\ &+ \frac{g}{4\pi M}\left[\sum_{j'\neq0,j_1-j}\phi^*_{j_1}\phi_{j_1-j'}\right]\phi_{j+j'}(\tau), \end{aligned} \tag{3}$$

where $\phi_j(\tau)$ is the jth Fourier component of the wavefunction $\phi(\theta,\tau)$ (that is, at momentum site j) and $M=Zk_L/2\pi$ (Z is the system size). The first term on the right-hand side corresponds to the single-particle evolution, which leads to momentum-space dynamical localization in the non-interacting QKR. The second and third terms correspond to diagonal (onsite attraction) and off-diagonal (infinite long-range hopping) interactions, respectively.

If only the diagonal interaction is considered, the free evolution yields $\phi_{-,j}=\phi_{+,j}\exp(i[\epsilon-\bar{k}j^2/2-g(2N_{\rm atom}-|\phi_{+,j}|^2)/4\pi M\bar{k}])$ and the nonlinear Anderson model becomes

$$V_j\bar{\phi}_j+\sum_{j'\neq0}K_{j'}\bar{\phi}_{j+j'}=\omega\bar{\phi}_j, \tag{4}$$

which has the same form as that for the non-interacting QKR, except that the onsite disorder is nonlinear with $V_j=\tan[\epsilon/2-\bar{k}j^2/4-gN_{\rm atom}/4\pi M\bar{k}+g|\sum_{j'}\bar{\phi}_{j+j'}(K_{j'}+\delta_{j,j'})|^2/8\pi M\bar{k}]$. Here $\bar{\phi}_j=(\phi_{-,j}+\phi_{+,j})/2$, hopping rates $K_j=\frac{1}{\sqrt{4M\pi}}\int d\theta e^{ij\theta}\tan\left[\frac{K}{2\bar{k}}\cos(\theta)\right]$ and energy $\omega=-K_0$. In the presence of infinite long-range hopping in the momentum space, the dynamics are much more complex, without an explicit relation between ϕ_- and ϕ_+. Such infinite long-range hopping destroys the quantum interference in the momentum space, leading to dynamical delocalization.

Data availability

The data that support the findings of this study are available via the Harvard Dataverse at https://doi.org/10.7910/DVN/9WLJXE. Any additional information is available from the corresponding authors upon reasonable request.

Code availability

The computer codes used for theoretical calculations in this study are available from C.Z. upon reasonable request.

References

41. Hansen, A. H. et al. Quantum degenerate mixture of ytterbium and lithium atoms. *Phys. Rev. A* **84**, 011606 (2011).
42. Roy, R., Green, A., Bowler, R. & Gupta, S. Rapid cooling to quantum degeneracy in dynamically shaped atom traps. *Phys. Rev. A* **93**, 043403 (2016).
43. Roy, R., Green, A., Bowler, R. & Gupta, S. Two-element mixture of Bose and Fermi superfluids. *Phys. Rev. Lett.* **118**, 055301 (2017).

Acknowledgements

We thank D. Weld, A. Rançon and V. Galitski for helpful discussions. Work at the University of Washington is supported by the Air Force Office of Scientific Research (FA9550-19-1-0012) and the National Science Foundation (PHY-1806212). K.C.M. is supported by an IC postdoctoral fellowship. The work at the University of Texas at Dallas is supported by the Air Force Office of Scientific Research (FA9550-20-1-0220), National Science Foundation (PHY-1806227 and PHY-2110212) and Army Research Office (W911NF-17-1-0128).

Author contributions

J.H.S.T., K.C.M. and X.T. performed the experimental measurements and data analysis. S.G. conceived the experiment and supervised the work. Y.S. and X.-W.L. performed the GP and HFB numerical simulations. C.Z. supervised the theoretical work. All the authors contributed to the preparation of the manuscript.

Competing interests

The authors declare no competing interests.

Additional information

Supplementary information The online version contains supplementary material available at https://doi.org/10.1038/s41567-022-01721-w.

Correspondence and requests for materials should be addressed to Chuanwei Zhang or Subhadeep Gupta.

Peer review information *Nature Physics* thanks Jakub Zakrzewski and the other, anonymous, reviewer(s) for their contribution to the peer review of this work.